PAFD: Phased Array Full-Duplex

Ehsan Aryafar[1] and Alireza Keshavarz-Haddad[2]
[1]Portland State University, Department of Computer Science, Portland, OR, 97201
[2]Shiraz University, School of Electrical and Computer Engineering, Shiraz, Iran

***Abstract*—We present the design and implementation of *PAFD*, a design methodology that enables full-duplex (FD) in hybrid beamforming systems with constant amplitude phased array antennas. The key novelty in *PAFD*'s design is construction of analog beamformers that maximize the beamforming gains in the desired directions while simultaneously reducing the self-interference (SI). *PAFD* is implemented on the WARP platform, and its performance is extensively evaluated in both indoor and outdoor environments. Our experimental results reveal that *(i)* *PAFD* sacrifices a few dB in beamfomring gain to provide large amounts of reduction in SI power; *(ii)* the reduction in SI is dependent on the number of phased array antennas and increases as the number of antennas increases; and *(iii)* finally, *PAFD* significantly outperforms half-duplex (HD) for small cells even in presence of high interference caused by uplink clients to the downlink clients. The gains increase with a larger array size or less multipath in the propagation environment.**

I. Introduction

Full-Duplex (FD) wireless communication, is the process of sending data at the same time and on the same frequency band. It has the potential to double the spectral efficiency of conventional half-duplex (HD) wireless systems. The main challenge to FD is self-interference (SI): a node's transmitting signal generates a significant amount of interference to its own receiver. Recent advances in RF and digital cancellation techniques [1], [2], [3], [4], [5], now allow us to reduce/eliminate the SI and build FD radios for small-antenna systems.

However, to address the exponential growth in data traffic, next generation wireless systems are expected to employ a very large number of antennas. For example, 3GPP has already decided to include 128-antenna base stations (BSs) for below 6GHz cellular systems and 1024-antenna BSs for mmWave cellular systems [6]. This increase in the number of antennas increases the beamforming gain and reduces the interference footprint, resulting in significant increase in the network capacity. To reduce the cost associated with having a separate Tx-Rx RF chain for each antenna element, hybrid beamforming has recently emerged as the de-facto architecture for next generation many-antenna systems. Each Tx-Rx RF chain in this architecture is connected to an antenna array (phased array). Fig. 1(a) shows the components of a conventional hybrid beamforming architecture.

The key question that we ask in this work is: *how to enable FD in such a hybrid beamforming architecture with phased array antennas?* The complexity of current SI cancellation techniques rapidly grows with the increase in number of antennas, making it infeasible to adopt these techniques in phased array systems. At the same time, the plurality of phased

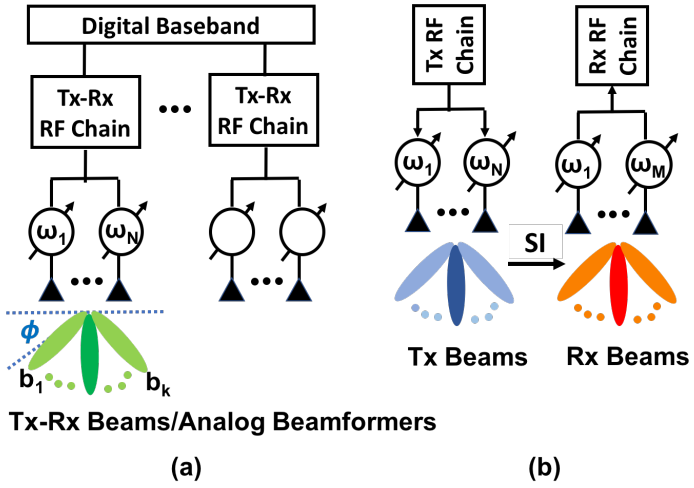

Fig. 1. **(a): A partially-connected hybrid beamforming architecture. Here each Tx-Rx RF chain is connected to a separate antenna array. The phase shifter on each antenna element i shifts the phase of the signal by multiplying the time domain RF signal by a complex coefficient ω_i with a constant amplitude across all the antennas; (b): *PAFD* uses separate Tx and Rx antenna arrays to reduce the SI. Further, the Tx (and/or Rx) beams are designed in such a way that not only they maximize the main beam gains in the desired directions, but they also reduce the SI.**

array antennas that are used to serve each client implies that the additional spatial resources can be used to reduce the SI.

In this work, we present the design and implementation of *PAFD*, the first FD design for hybrid beamforming systems with phased array antennas. *PAFD* uses separate Tx and Rx antenna arrays to reduce the SI (Fig. 1(b)). Note that the processing complexity (and price) of a transceiver lies predominantly in its RF chains and not its passive antennas. Hence, leveraging additional arrays, while a *form factor* issue for low frequency mobile devices, is not an obstacle for BSs or high frequency (*e.g.* mmWave) wireless devices, which are where we expect FD to be predominantly employed.

The key idea behind *PAFD*'s design is to construct the Tx (or/and Rx) analog beamformers of each phased array in such a way that not only they maximize the main beam gains in the desired directions, but they also reduce the SI (Fig. 1(b)). We show that *PAFD*'s design provides large amounts of reduction in SI with several key advantages: (i) it eliminates the need for any form of adaptive (real time) analog cancellation, which lack scalability to phased array systems due to cost and complexity issues; (b) it easily scales to multiple Tx and/or Rx RF chain hybrid beamforming systems, thereby enabling the

co-existence of MIMO with FD; and (iii) it is agnostic of the underlying digital beamforming performed on the baseband of a hybrid beamforming architecture. Thus, *PAFD* can operate on top of conventional MU-MIMO algorithms (*e.g.* zero-forcing beamforming [7]) without affecting their operation.

PAFD is implemented on the WARP platform and its performance is extensively evaluated in both indoor and outdoor environments. Our experimental results reveal that: *(i)* in outdoor deployments and with a linear antenna setup, PAFD reduces the beamforming gain by less than 2 dB , but compensates for that by providing 40 dB of reduction in SI. Further, *PAFD*'s beamforming and SI reduction gains improve as the number of phased array antennas increases; *(ii)* the strong non-line-of-sight (nLoS) components of the SI channel in an indoor environment, reduce the SI reduction gains of PAFD. However, PAFD can still reduce the SI by more than 35 dB in indoor multipath rich environments. Further, due to reflections and multipath scattering the gap in beamforming gain between PAFD and standard analog beams (that only maximize the beamforming gains in the desired directions) disappears; and *(ii) PAFD* provides significant capacity gains compared to HD systems in single cell environments even in presence of interference caused by UL clients to the DL clients. The gains increase with a larger array size and/or with less multipath.

The rest of this paper is organized as follows. We discuss the background and related work in Section II. Section III describes the problem formulation. Section IV develops an analog beamformer design method for *PAFD*. Section V describes its implementation followed by detailed evaluation in Section VI. Finally, we conclude the paper in Section VII.

II. Background and Related Work

A. Preliminaries

Phased Arrays. Fig. 1(a) depicts the various components of a conventional hybrid beamforming architecture termed *partially-connected structure*. Here each Tx-Rx RF chain is connected to a fixed set of antenna elements, feeding them with the same RF signal. These antenna arrays are referred to as phased arrays. The phase shifter on each antenna element i shifts the phase of the signal by multiplying the time domain RF signal by a complex coefficient ω_i which has a *constant amplitude across all the phased array antennas.* In practice, a phase shifter is a discrete/quantized component with a few bits of resolution. For example, the phase of a 2-bit phase shifter can only be selected from the set $\{0^\circ, 90^\circ, 180^\circ, 270^\circ\}$.

Analog Beamformers and Codebook. In a phased array, a set of pre-determined beam patterns (*e.g.*, b_1, ..., b_K in Fig. 1(a)) is available. Each of these beams is realized by an appropriate setting of phase shifts across all the antennas. The vector of phase shifts across all the phase array antennas that realizes a particular beam pattern (*e.g.*, b_k) is referred to as an analog beamformer, and the set of all these analog beamformers is referred to as a codebook.

Each beam b_k has a main lobe of maximum gain in a particular direction ϕ_k[1] (Fig. 1(a)) and side lobes representing leakage of energy in all the other directions. The increase in the number of antenna elements, increases the array gain and reduces the beamwidth of the main lobe. For example in a uniform linear array (ULA) with N antennas and $\frac{\lambda}{2}$ spacing distance (λ is the carrier wavelength), the main lobe beamforming gain is equal to $10\times\log_{10}^{N}$ (in dB) with $\frac{102}{N}$ (in degrees) half power beamwidth [8]. Analog beamformers in conventional phased arrays (*e.g.*, below 6GHz cellular BSs, conventional mmWave products [9]) typically provide a 120° coverage area (*e.g.*, $\phi \in [30^\circ\ 150^\circ]$ in Fig. 1(a)). Thus, the total number of required analog beams to provide a 120° coverage area would be approximately equal to $\frac{120\times N}{102}$ (assuming a maximum 3 dB loss between adjacent beams).

B. Related Work

Full Duplex. Recent works have proposed *antenna*, *analog*, and *digital* cancellation techniques to enable FD with a small number of antennas. Antenna cancellation arranges Tx and Rx antennas in a manner such that the SI is reduced at Rx antennas [1], [3], [4]. Analog and digital cancellation [2], [5], [10] require knowledge of the transmitted signal and the SI channel to create an inverse copy of the SI signal in the RF and digital domains, respectively. The complexity of all these techniques significantly increases with the increase in the number of antennas, making it infeasible to adopt these techniques in phased array based systems studied in this paper.

Massive MIMO. The significant performance gains of large-scale MU-MIMO systems have been demonstrated through experimental research platforms such as Argos [11], BigStation [12], and Hekaton [13]. In Argos and BigStation, each Tx-Rx RF chain is connected to a separate antenna element. Hekaton shows the benefits of large-scale MU-MIMO through a partially-connected hybrid beamforming architecture in which each Tx-Rx RF chain is connected to a phased array. All these platforms operate in a half-duplex mode. Softnull [14] presents a digital beamforming solution to enable FD in the Argos massive MIMO platform. Softnull requires a separate Tx-Rx RF chain for each antenna element. In contrast, $PAFD$ is designed for the more conventional hybrid beamforming architecture with phased array antennas.

Radar Beam Synthesis. The problem of radar beam synthesis to achieve a desired Tx or Rx beampattern in the *far-field* has been studied in the literature [15], [16], [17]. However, the far-field range condition [18] would not hold for a FD radio even in mmWave frequencies due to the proximity of Tx and Rx antenna arrays. This makes it infeasible to apply these techniques to the FD problem studied in this paper.

III. Problem Formulation

A. System Model

A phased array applies a vector of beamforming weights in the RF domain to each of its antenna elements to create a directional Tx/Rx beam pattern. Let $\omega_i \in \mathbb{C}$ denote the

[1]For ease of discussion we only consider the Azimuth plane.

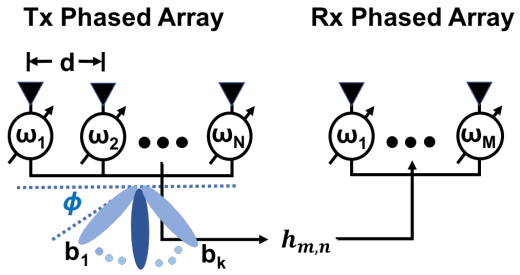

Fig. 2. **Configuration of Tx and Rx ULA antennas. The phase shifter on each antenna element has a constant amplitude across all the antennas but with different phases, *i.e.*, $\omega_i = \sqrt{P}e^{j\Omega_i}$. The SI channel between Rx antenna element m and Tx antenna element n is denoted by $h_{m,n}$.**

phase shifter weight for antenna element i and $\mathbf{w} \in \mathbb{C}^{N\times 1}$ the corresponding Tx weight vector (also referred to as Tx analog beamformer) for an N antenna Tx phased array. Let $\mathbf{w}_{Rx} \in \mathbb{C}^{M\times 1}$ denote the corresponding Rx weight vector for an M antenna Rx phased array. We consider a constant amplitude phased array in which the phase shifter on each antenna element has a constant amplitude across all the antennas but with different phase values, *i.e.*, $\omega_i = \sqrt{P} \times e^{j\Omega_i}$ where P is the transmission power (when Tx beamforming) or Rx gain (when Rx beamforming). For ease of discussion, we consider a *narrowband* system, isotropic antennas, and focus on uniform linear arrays (ULAs) with equal spacing distance d. Fig. 2 depicts a baseline *PAFD* architecture with an N antenna Tx phased array and an M antenna Rx phased array.

SI Signal Characterization. The received baseband signal y at the Rx phased array is given by:

$$y = \mathbf{w}_{Rx}^T \mathbf{H} \mathbf{w} x + z \tag{1}$$

here ^{T} denotes the transpose operator, $x \in \mathbb{C}$ is the transmitted symbol, $\mathbf{H} = [h_{mn}]_{M\times N}$ is the SI channel matrix between Rx and Tx antenna elements (*i.e.*, $h_{m,n} \in \mathbb{C}$ is the SI channel coefficient between Rx antenna element m and Tx antenna element n), and z represents the circularly symmetric additive white Gaussian noise at the receiver. Without loss of generality, we assume $|x|^2 = 1$. Hence, the resulting SI power at the Rx phased array is equal to $|\mathbf{w}_{Rx}^T \mathbf{H} \mathbf{w}|^2 = (\mathbf{w}_{Rx}^T \mathbf{H} \mathbf{w})^* \mathbf{w}_{Rx}^T \mathbf{H} \mathbf{w}$, where * denotes the conjugate transpose.

Far-Field Beampattern Characterization. Analog beamformers in conventional phased arrays are designed to provide a high beamforming gain in a desired direction. According to [8], the far-field Tx array-factor (gain at spatial direction ϕ in Fig. 2) for a given Tx analog beamformer ($\mathbf{w}$) is:

$$AF(\phi) = \sum_{i=1}^{N} e^{j2\pi i d \frac{\cos(\phi)}{\lambda}} \times \omega_i = \mathbf{a}(\phi)\mathbf{w} \tag{2}$$

where

$$\mathbf{a}(\phi) = [e^{j2\pi d \frac{\cos(\phi)}{\lambda}} \quad ... \quad e^{j2\pi N d \frac{\cos(\phi)}{\lambda}}] \tag{3}$$

The corresponding far-field Tx beampattern at spatial direction ϕ is then given by [8], [17]:

$$|AF(\phi)|^2 = |\mathbf{a}(\phi)\mathbf{w}|^2 \tag{4}$$

Note that $\mathbf{a}(\phi)$ is continuous in phase. It can be expressed as a discrete angle vector by dividing the desired coverage area (*e.g.* [30° 150°]) to K angles and be written as

$$\mathbf{a}_k = \mathbf{a}(\phi_k), \quad k = 1, ..., K \tag{5}$$

B. Analog Beamformer Design Problem Formulation

PAFD pursues two objectives in its construction of analog beamformers: *(i)* reduce the SI at the Rx phased array, and *(ii)* provide a high Tx beamforming gain in the desired directions. In our problem formulation we consider the problem of Tx analog beamformer design and construct the Tx beams in such a way that the SI is reduced for any Rx analog beamformer. Similar methods can be used to construct the Rx analog beamformers and further reduce the SI.

Let $\mathbf{h}_m = [h_{m,1}, ..., h_{m,N}]$ denote the SI channel vector between the Rx antenna element m and the Tx antenna elements. Following the methodology in Section III-A, the RF domain Tx signal energy at Rx antenna element m would be equal to $|\mathbf{h}_m \mathbf{w}|^2$. Our goal to reduce the SI at the Rx phased array is to minimize the *total* RF domain SI power. Our choice is motivated by two observations: *(i)* minimizing the total SI power reduces the per-element RF domain SI power. This results in reduced SI for any Rx analog beamformer ($\mathbf{w}_{Rx}$), and *(ii)* minimizing the total SI gives the analog beamformer more freedom to create nulls, *e.g.*, instead of creating a null at a specific antenna element location, the method can place the null in such a way that the SI is reduced across multiple antenna locations.

Let d_g denote the desired array-factor gain, and $c_1, c_2 \in \mathbb{R}_+$ as inputs to provide different tradeoffs in SI reduction and beamforming gain. Then, for each direction ϕ_k, we seek to solve the following overall optimization problem:

$$\mathcal{P}_1 : \begin{cases} \min\limits_{\mathbf{w}} & \sum\limits_{m=1}^{M} c_1(|\mathbf{h}_m \mathbf{w}|)^2 + c_2(d_g - |\mathbf{a}_k \mathbf{w}|)^2 \\ s.t. & |\omega_i|^2 = P \qquad \forall\ i = 1, ..., N \end{cases} \tag{6}$$

In the above formulation, we seek to find a Tx analog beamformer ($\mathbf{w}$) with a low residual SI at the Rx phased array and a high beamforming gain in the direction ϕ_k. The first term in Eq. (6) aims to reduce the total SI. The second term aims to provide a high beamforming gain in the spatial direction ϕ_k. From Eq. (2), it follows that the $AF(\phi_k)$ is maximized when $\arg(\omega_i) = -2\pi i d \frac{\cos(\phi_k)}{\lambda}$ ($\forall\ i = 1, ..., N$) and the maximum array-factor gain for any direction ϕ_k is $\sqrt{P}N$. Thus, we can set d_g to $\sqrt{P}N$. We can easily absorb c_1 and c_2 in the two terms of the objective function by scaling the $\mathbf{h}_m, d_g$, and $\mathbf{a}_k$ input variables. For ease of discussion, for the rest of this paper we assume $c_1 = c_2 = 1$.

IV. Analog Beamformer Design Method

The optimization problem in $\mathcal{P}_1$ is non-convex (and thus difficult in general) because of the constant amplitude constraint. As shown in [17], it is more convenient to rewrite the objective function of Eq. (6) as

$$\sum_{m=1}^{M} (\mathbf{h}_m \mathbf{w})^2 + (d_g e^{j\theta_0} - \mathbf{a}_k \mathbf{w})^2 \tag{7}$$

where $\theta_0 = \arg\{\mathbf{a}_k \mathbf{w}\}$. Since $\mathbf{w}$ is unknown, θ_0 is also unknown. This problem can be resolved by an iterative method ([17], [19]). The method minimizes Eq. (7) by iteratively fixing the value of θ_0 and minimizing with respect to $\mathbf{w}$, and then fixing $\mathbf{w}$ and minimizing with respect to θ_0. This iterative method is monotonically decreasing and converges to a final value [17], [19]. Hence, we need to solve the following constrained problem for a fixed value of θ_0:

$$\mathcal{P}_2 : \begin{cases} \min\limits_{\mathbf{w}} & \sum\limits_{m=0}^{M} (d_m e^{j\theta_m} - \mathbf{b}_m \mathbf{w})^2 \\ s.t. & |\omega_i|^2 = P \qquad \forall\ i = 1, ..., N \end{cases} \tag{8}$$

with

$$\begin{cases} \mathbf{b}_m = \mathbf{a}_k, \quad d_m = d_g & m = 0 \\ \mathbf{b}_m = \mathbf{h}_m, \quad d_m = 0, \quad \theta_m = 0 & \forall\ m = 1, ..., M \end{cases} \tag{9}$$

Now, let us define the following variables:

$$\mathbf{d} = \begin{bmatrix} d_0 e^{j\theta_0} \\ ... \\ d_M e^{j\theta_M} \end{bmatrix}, \quad \mathbf{B} = \begin{bmatrix} \mathbf{b}_0 \\ ... \\ \mathbf{b}_M \end{bmatrix} \tag{10}$$

Problem $\mathcal{P}_2$ can be written in terms of $\mathbf{d}$ and $\mathbf{B}$ as:

$$\mathcal{P}_3 : \begin{cases} \min\limits_{\mathbf{w}} & ||\mathbf{d} - \mathbf{B}\mathbf{w}||_2^2 \\ s.t. & |\omega_i|^2 = P \qquad \forall\ i = 1, ..., N \end{cases} \tag{11}$$

We propose a semidefinite relaxation (SDR) method to solve the problem in $\mathcal{P}_3$. Let $\Re$ and $\Im$ denote the real and imaginary operators, respectively. First, we turn the problem $\mathcal{P}_3$ into the following real-valued problem

$$\mathcal{P}_4 : \begin{cases} \min\limits_{\mathbf{w}'} & ||\mathbf{d}' - \mathbf{B}'\mathbf{w}'||_2^2 \\ s.t. & \mathbf{w}'^T \mathbf{Q}'_n \mathbf{w}' = P \qquad \forall\ n = 1, ..., N \end{cases} \tag{12}$$

where

$$\mathbf{d}' = \begin{bmatrix} \Re\{\mathbf{d}\} \\ \Im\{\mathbf{d}\} \end{bmatrix}, \mathbf{B}' = \begin{bmatrix} \Re\{\mathbf{B}\} & -\Im\{\mathbf{B}\} \\ \Im\{\mathbf{B}\} & \Re\{\mathbf{B}\} \end{bmatrix}, \mathbf{w}' = \begin{bmatrix} \Re\{\mathbf{w}\} \\ \Im\{\mathbf{w}\} \end{bmatrix} \tag{13}$$

here $\mathbf{d}' \in \mathbb{R}^{2(M+1)\times 1}$, $\mathbf{B}' \in \mathbb{R}^{2(M+1)\times 2N}$, $\mathbf{w}' \in \mathbb{R}^{2N\times 1}$, and $\mathbf{Q}'_n$ are N diagonal matrices of dimension $2N \times 2N$

$$\mathbf{Q}'_n(i,i) = \begin{cases} 1 & \text{if } i = n \text{ or } i = n+N \\ 0 & \text{otherwise} \end{cases} \tag{14}$$

Next, we introduce an auxiliary variable $t \in \mathbb{R}$ and turn problem $\mathcal{P}_4$ to

$$\mathcal{P}_5 : \begin{cases} \min\limits_{\mathbf{w}', t} & ||t\mathbf{d}' - \mathbf{B}'\mathbf{w}'||_2^2 \\ s.t. & t^2 = 1, \quad \mathbf{w}'^T \mathbf{Q}'_n \mathbf{w}' = P \quad \forall\ n = 1, ..., N \end{cases} \tag{15}$$

Problem $\mathcal{P}_5$ is equivalent to problem $\mathcal{P}_4$ in the sense that if $(\mathbf{w}'^o, t^o)$ is an optimal solution to $\mathcal{P}_5$, then $\mathbf{w}'^o$ (-$\mathbf{w}'^o$) is an optimal solution to $\mathcal{P}_4$ when $t^o = 1$ ($t^o = -1$). The objective function in problem $\mathcal{P}_5$ can be written as:

$$\begin{aligned} ||t\mathbf{d}' - \mathbf{B}'\mathbf{w}'||_2^2 &= (t\mathbf{d}' - \mathbf{B}'\mathbf{w}')^T (t\mathbf{d}' - \mathbf{B}'\mathbf{w}') \\ &= [\mathbf{w}'^T \ t] \begin{bmatrix} \mathbf{B}'^T\mathbf{B}' & -\mathbf{B}'^T\mathbf{d}' \\ -\mathbf{d}'^T\mathbf{B}' & ||\mathbf{d}'||^2 \end{bmatrix} \begin{bmatrix} \mathbf{w}' \\ t \end{bmatrix} \end{aligned} \tag{16}$$

Now, let us define the following variables:

$$\mathbf{w}'' = \begin{bmatrix} \mathbf{w}' \\ t \end{bmatrix}, \quad \mathbf{B}'' = \begin{bmatrix} \mathbf{B}'^T\mathbf{B}' & -\mathbf{B}'^T\mathbf{d}' \\ -\mathbf{d}'^T\mathbf{B}' & ||\mathbf{d}'||^2 \end{bmatrix} \tag{17}$$

& $N+1$ diagonal matrices of dimension $(2N+1)\times(2N+1)$

$$\mathbf{Q}''_n(i,i) = \begin{cases} 1 & \text{if } n \neq N+1 \text{ and } i = n \\ 1 & \text{if } n \neq N+1 \text{ and } i = n+N \\ 1 & \text{if } n = N+1 \text{ and } i = 2N+1 \\ 0 & \text{otherwise} \end{cases} \tag{18}$$

Then problem $\mathcal{P}_5$ can be turned to

$$\mathcal{P}_6 : \begin{cases} \min\limits_{\mathbf{w}''} & \mathbf{w}''^T \mathbf{B}'' \mathbf{w}'' \\ s.t. & \mathbf{w}''^T \mathbf{Q}''_n \mathbf{w}'' = P \qquad \forall\ n = 1, ..., N \\ & \mathbf{w}''^T \mathbf{Q}''_n \mathbf{w}'' = 1 \qquad n = N+1 \end{cases} \tag{19}$$

Problem $\mathcal{P}_6$ is a homogeneous Quadratic Constrained Quadratic Problem (QCQP). Since $\mathbf{B}''$ and $\mathbf{Q}''$ are real symmetric matrices and $\mathbf{w}'' \in \mathbb{R}^{(2N+1)\times 1}$ we have

$$\begin{aligned} \mathbf{w}''^T \mathbf{B}'' \mathbf{w}'' &= \text{Tr}(\mathbf{w}''^T \mathbf{B}'' \mathbf{w}'') = \text{Tr}(\mathbf{B}'' \mathbf{w}'' \mathbf{w}''^T) \\ \mathbf{w}''^T \mathbf{Q}'' \mathbf{w}'' &= \text{Tr}(\mathbf{w}''^T \mathbf{Q}'' \mathbf{w}'') = \text{Tr}(\mathbf{Q}'' \mathbf{w}'' \mathbf{w}''^T) \end{aligned} \tag{20}$$

where *Tr* is the trace function. Thus, by introducing a new variable $\mathbf{W} = \mathbf{w}''\mathbf{w}''^T$ and noting that $\mathbf{W} = \mathbf{w}''\mathbf{w}''^T$ is equivalent to $\mathbf{W}$ being a rank one symmetric positive semidefinite (PSD) matrix, we obtain the following equivalent formulation of problem $\mathcal{P}_6$:

$$\mathcal{P}_7 : \begin{cases} \min\limits_{\mathbf{W} \in \mathbb{S}^{2N+1}} & \text{Tr}(\mathbf{B}''\mathbf{W}) \\ s.t. & \text{Tr}(\mathbf{Q}''_n \mathbf{W}) = P \qquad \forall\ n = 1, ..., N \\ & \text{Tr}(\mathbf{Q}''_n \mathbf{W}) = 1 \qquad n = N+1 \\ & \mathbf{W} \succeq \mathbf{0}, \quad \text{rank}(\mathbf{W}) = 1 \end{cases} \tag{21}$$

Here $\mathbb{S}^{2N+1}$ denotes the set of all real symmetric $(2N+1)\times(2N+1)$ matrices and $\mathbf{W} \succeq \mathbf{0}$ indicates that $\mathbf{W}$ is PSD. The

only difficult constraint in problem $\mathcal{P}_7$ is the rank constraint. By dropping this constraint we obtain the following relaxation:

$$\mathcal{P}_8 : \begin{cases} \min\limits_{\mathbf{W}\in\mathbb{S}^{2N+1}} & \text{Tr}(\mathbf{B}''\mathbf{W}) & \\ s.t. & \text{Tr}(\mathbf{Q}_n''\mathbf{W}) = P & \forall\ n = 1, ..., N \\ & \text{Tr}(\mathbf{Q}_n''\mathbf{W}) = 1 & n = N+1 \\ & \mathbf{W} \succeq \mathbf{0} & \end{cases} \quad (22)$$

which is called a semidefinite relaxation (SDR) and is an instance of semidefinite programming. Problem $\mathcal{P}_8$ is convex and can be solved in polynomial time with readily available software such as CVX. There is, however, a price in turning the non-convex problem in $\mathcal{P}_7$ to the polynomial-time solvable problem in $\mathcal{P}_8$ and that is the *rank* of the output of the relaxed solution may be high ($>$1). We use standard SDP methods to encourage low rank solutions [20] and then approximate a feasible rank one solution from the output of problem $\mathcal{P}_8$ [21]. Finally, in order to accommodate phase quantization in real-world phased arrays, we round each *PAFD* weight to the nearest available quantized phase shift.

V. Implementation

We have evaluated the performance of *PAFD* in terms of its beamforming gain and SI reduction using the WARP FPGA boards. Our implementation is based on the WARPLab framework. In this framework, all WARP boards are connected to a host PC through an Ethernet switch. The host PC is responsible for baseband PHY signal processing, while WARP boards act as RF front-ends to send/receive packets over the air. We employ up to 4 WARP boards each with 4 RF chains to construct up to a 16 antenna (8Tx-8Rx) FD BS. We also build FD BSs with a lower number of antennas (*e.g.*, 4Tx-4Rx, 8Tx-4Rx), in order to evaluate the impact of antenna size on our performance metrics. All of our experiments were conducted in the 2.4 GHz band channel 14 (least external interference) and we used 3dBi dipole antennas. Unless otherwise specified, we place all the antennas in a ULA manner with half a wavelength spacing distance. We employ another two WARP boards to emulate up to 8 single-antenna clients.

Phased Array Implementation. Commercial phased array products (*e.g.*, [9]) provide only discrete phase shifts on each antenna element. To capture this in our implementation, we construct a digital phased array antenna using the WARP boards. In our implementation, we emulate the phase quantization by selecting the phase shift that is applied to each antenna element from a discrete set of values. The number of these quantized phase shifts is a hardware-specific value. Similar to [9], we assume a 5-bit phase shifter resolution, *i.e.*, the phase shifts can be selected from the set $\{0, \frac{1\times2\pi}{32}, ..., \frac{31\times2\pi}{32}\}$. We also normalize the transmit power of each emulated phased array to be equal to that of a single WARP RF chain.

Phased Array Calibration. In phased array antennas, the transmit phase at each antenna element is known at the phased array. However, since in our implementation we use a different RF chain for each antenna element, hardware differences across the radios introduce varying phase offsets between the antennas. To address the issue, we apply the phase calibration mechanism of [13] to all the antennas to synchronize the phase of all the antenna elements. First, we randomly select a *lead* antenna and transmit a preamble symbol on that antenna element. Every other antenna element uses its received phase information, along with its known physical location to derive its own phase offset from the lead antenna. It then compensates for this phase offset in all subsequent transmissions. This calibration is done for both Tx and Rx phase arrays.

Half-Duplex DFT CodeBook. We use the standard Discrete Fourier Transform (DFT) codebook [22] as the baseline in our half-duplex (HD) implementation. For a given direction ϕ_k, the DFT codebook specifies the phase shifts that should be applied to each antenna element to maximize the beamforming gain in that direction. As discussed in Section II-A, the number of codebook elements depends on the desired coverage area and the number of antenna elements N. Similar to *PAFD*, each DFT weight (phase shift) is rounded to the nearest available quantized phase shift.

SI Channel Estimation. *PAFD* requires the SI channel information in its construction of analog beamformers ($\mathcal{P}_1$). Recent works have proposed several solutions to obtain the channel in hybrid arrays. We adopt a solution similar to the one proposed in [23] for channel estimation. In a nutshell, the solution sends a small series of beamformed reference signals across all Tx antennas and leverages the feedback to reconstruct the channel. In *PAFD*, the SI channel is between the Tx and Rx antennas of the same device, hence there is no over-the-air feedback overhead. Moreover, the SI channel in *PAFD* is dominated by the LoS component and hence changes very slowly over time. In our experiments, we obtain the SI channel information only once during the setup and use that for the rest of the duration of the experiment (a few hours).

VI. Performance Evaluation

In this section, we evaluate the performance of *PAFD* in several aspects. First, we consider how the *number of antenna elements in Tx and/or Rx phased arrays* and *the antenna structure* impact the beamforming gains and SI reduction capabilities of *PAFD*. Second, we study the impact of the propagation environment on these tradeoffs. Next, we study the capacity gains that *PAFD* can deliver to clients. Finally, we extend our evaluation to MIMO (multiple Tx & Rx phased arrays). In all, we compare the performance of *PAFD* against a HD phased array system that employs the DFT codebook.

A. Experimental Setup

Unless otherwise specified, we consider a ULA antenna structure (Fig. 3(a)) with one Tx phased array and one Rx phased array. We use N antennas for our Tx phased array and M antennas for our Rx phased array. For a fair comparison, we use the same antenna structure for both FD and HD systems.

SI Measurement Setup. We take the following steps to measure the reduction in SI with different analog beamformers. First, we transmit with the full power of a single RF chain

P on Tx antenna 1 (Fig. 3(a)) and measure the amount of SI at each of the M Rx antenna elements. Next, we apply the desired phase shift across each of the N Tx antenna elements (while equally splitting the total power P across them), and re-measure the SI. We calculate the reduction in SI by subtracting the first SI measurement from the second SI measurement at each Rx antenna element, and averaging them over all the Rx antennas. Each of our SI data points is an average of 10 such measurements.

Set of Desired Directions (Angles). We construct 4 and 8 antenna Tx phased arrays. Similar to a conventional cellular BS or a mmWave radio [9], we consider a 120° desired coverage area (*i.e.*, Azimuth angle $\phi \in [30°150°]$). With 4 and 8 Tx antennas, the half power beamwidths are approximately 25° and 12°, respectively. Hence, we choose the sets of desired directions as $\{30°, 60°, 90°, 120°, 150°\}$ and $\{30°, 45°, 60°, 75°, 90°, 105°, 120°, 135°, 150°\}$ for 4 and 8 antenna Tx phased arrays, respectively. In other words, we construct our analog beamformers to provide maximum beamforming gains in these directions.

B. Number of Antenna Elements

Analog beamformers in *PAFD* are designed to maximize the beamforming gain in the desired directions while simultaneously minimizing the SI. This reduces the beamforming gain compared to only maximizing the beamforming gain (*i.e.*, the DFT codebook). In this section we characterize the beamforming gain and SI reduction characteristics of *PAFD* for different numbers of antennas in Tx and Rx phased arrays.

Scenario. We conduct our experiments in an outdoor deployment as depicted in Fig. 3(b). A single antenna client rotates around the BS in a circle with a $5m$ radius. We take measurements at $\phi = [30°\ 60°\ 90°\ 120°\ 150°]$ and $\phi = [30°\ 45°\ 60°\ 75°\ 90°\ 105°\ 120°\ 135°\ 150°]$ for 4 and 8 antenna Tx phased arrays, respectively. We first measure the beamforming gain for each client location when phases are set according to the DFT codebook to point towards the client location. We also measure the corresponding reduction in SI power. Next, we measure the beamforming gain at the same location and the reduction in SI when phases are set according to $PAFD$.

Beamforming Gain. Figs. 3(c) and 3(d) depict the loss in beamforming gain of *PAFD* with respect to the corresponding DFT beamformer for 4 and 8 Rx antenna phased arrays, respectively. In each figure, we consider both cases of having 4 or 8 Tx antenna phased arrays. We observe that *PAFD* reduces the beamforming gain in the desired directions in all the experiments. The loss in beamforming gain is higher with a higher number of Rx antennas or a lower number of Tx antennas. We observe that this loss is minimum when we have 8 Tx antennas and 4 Rx antennas with an average of 0.58 dB, and is maximum when we have 4 Tx antennas and 8 Rx antennas with an average of 2.1 dB.

When the number of Tx phased array antennas is higher than the number of Rx phased array antennas, there are many degrees of freedom to reduce the total SI. As a result, the loss in beamforming gain would be low. In contrast, when the number of Tx phased array antennas is lower, the number of degrees of freedom reduces. This increases the loss in beamforming gain. We next study whether the reduction in SI is worth the loss in beamforming gain.

SI Reduction. Figs. 3(e) and 3(f) depict the reduction in SI for 4Tx-4Rx and 8Tx-8Rx phased array antenna setups, respectively. In each figure we plot the reduction in SI when phases are set according to the DFT codebook and *PAFD*. The DFT codebook adjusts the phases to obtain single-lobe beams with dominant directions. This also reduces the SI in the direction of the Rx phased array. Figs. 3(e) and 3(f) show that the average reduction in SI when phases are set according to the DFT codebook is 14.6 dB and 15.6 dB in 4Tx-4Rx and 8Tx-8Rx phased array antenna setups, respectively.

In contrast, *PAFD* adjusts the phases to simultaneously maximize the beamforming gain and reduce the SI. We observe that when phases are set according to *PAFD*, the average reduction in SI is 41.4 dB and 45 dB in 4Tx-4Rx and 8Tx-8Rx phased array antenna setups, respectively. We observe that the reduction in SI increases with an increasing number of antennas in a ULA antenna setup. This is because in a linear arrangement of antennas (Fig. 3(a)), the SI channel to Rx antennas would be highly correlated. This makes it easier for *PAFD* to reduce the overall SI and increase the beamforming gain as the size of the linear array increases. We will discuss this issue in more detail in the next section.

Findings: In outdoor environments and with a ULA antenna setup, PAFD reduces the beamforming by 0.6-2.1 dB compared to the DFT codebook, but compensates for that by providing 25-30 dB additional reduction in SI. Further, PAFD's performance improves as the number of Tx antennas increases.

C. Antenna Structure

In this section, we change the Tx and Rx antenna structures to the T structure depicted in Fig. 3(a) and study the resulting impact on the beamforming and SI characteristics of *PAFD*. We consider the same outdoor deployment and measurement setup that was discussed in the previous section.

Intuitively, we expect that *PAFD* will perform the best when the SI channel is concentrated within a few dominant directions (*i.e.*, eigenchannels). Recent theoretical works (*e.g.*, [24]) have shown that as the spread of the angles-of-departure from the Tx antennas to Rx antennas is decreased (*e.g.*, in a ULA antenna setup), the signals received at different Rx antennas become more correlated. This results in a few dominant directions, which is the desirable situation for *PAFD*. In a T antenna structure, the spread of the angles-of-departure increases which can reduce the performance of *PAFD*.

Beamforming Gain. Fig. 3(g) depicts the loss in beamforming gain with respect to the DFT codebook. Note that unlike *PAFD*, the beamforming gain of the DFT codebook only depends on the client location and is not dependent on the Rx phased array antenna setup (*i.e.*, its beamforming gain remains the same for both ULA and T antenna setups).

We consider 4 and 8 antenna Tx phased arrays, and a 4 antenna Rx phased array. Our results show that *PAFD*

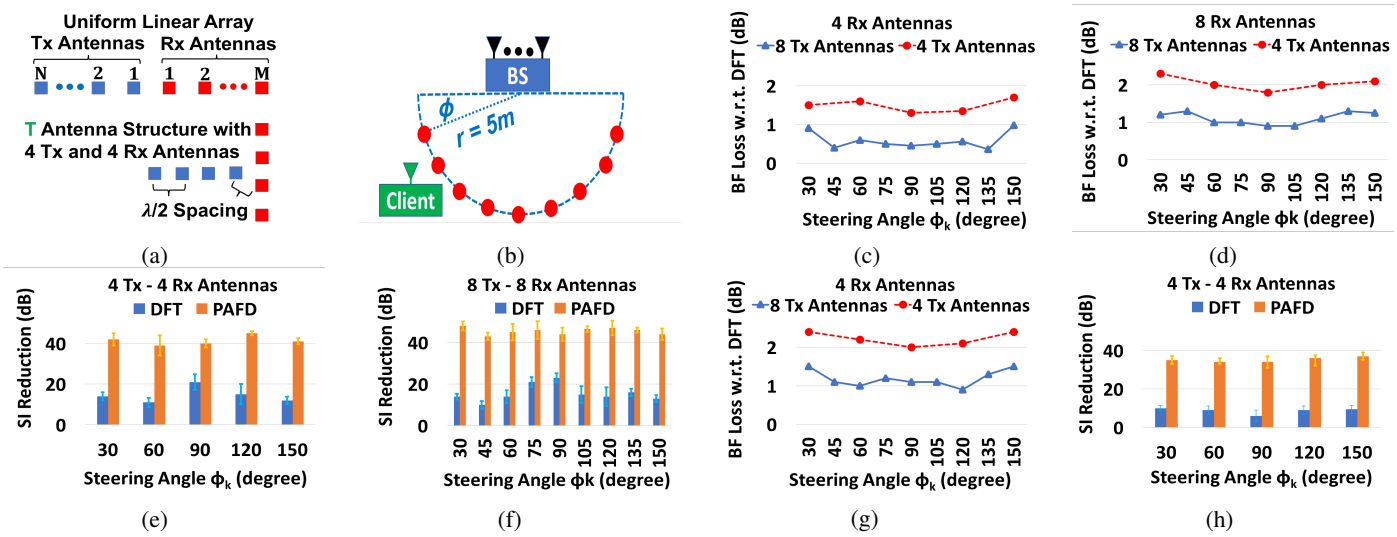

Fig. 3. **Outdoor measurement results. (a): Uniform linear array (ULA) and T antenna structures, (b): Beamforming gain and SI reduction measurement setup, (c): *PAFD*'s beamforming loss with respect to the DFT codebook for a 4 Rx antenna phased array, (d): *PAFD*'s beamforming loss with respect to the DFT codebook for an 8 Rx antenna phased array, (e): Reduction in SI for a 4Tx-4Rx phased array antenna setup, (f): Reduction in SI for an 8Tx-8Rx phased array antenna setup, (g): *PAFD*'s beamforming loss with respect to the DFT codebook for a 4 Rx antenna phased array with a T structure, (h): Reduction in SI for a 4Tx-4Rx phased array with a T structure.**

reduces the average beamforming gain for 8 Tx and 4 Tx antenna phased arrays by 1.2 dB and 2.2 dB, respectively. This is approximately 0.7 dB more loss in beamforming gain compared to the results that were achieved with the ULA antenna setup (Fig. 3(c)). Next, we investigate how the increased angles-of-departure impact the reduction in SI.

SI Reduction. Fig. 3(h) depicts the reduction in SI for a 4Tx-4Rx T structure phased array antenna setup. Note that SI measurements depend on the exact location of Rx phased array antennas. Hence, both *PAFD* and DFT would be impacted by the antenna structure. We observe that the DFT codebook reduces the SI by an average of 8.5 dB. This is 6 dB increase in SI compared to the results that were achieved with the ULA antenna setup (Fig. 3(e)). In *PAFD*, the average reduction in SI is 35 dB, which is an additional 6.4 dB SI compared to the ULA antenna setup (Fig. 3(e).

Findings: The increased spread of angles-of-departures from Tx antennas to Rx antennas in a T antenna structure, reduces the beamforming and SI reduction characteristics of PAFD. Changing the 4Tx-4Rx antenna structure from ULA to T, reduces the beamforming gain of PAFD by 0.7 dB and increases the SI by 6.4 dB.

D. Impact of Scattering

The scattering environment impacts the beamforming and SI characteristics of *PAFD*. In this section, we repeat the measurement scenario that was described in Section VI-B (and Fig. 3(b)) in an indoor multipath rich environment.

Beamforming Gain. Fig. 4(a) depicts the beamforming loss with respect to the DFT codebook in a 4 Rx antenna phased array setup. Unlike the outdoor results of Section VI-B in which *PAFD* consistently achieved a lower beamforming gain compared to the DFT codebook, we observe that in several directions loss in beamforming gain is negative (*i.e.*, *PAFD* provides a higher beamforming gain than the DFT codebook). Further, the average beamforming loss with respect to the DFT codebook reduces to 0.4 dB (from 1.6 dB in Fig. 3(c)) and 0.2 dB (from 0.6 dB in Fig. 3(c)) with 4 and 8 Tx phased array antenna setups, respectively.

This is because in an indoor multipath rich environment, the resulting energy at the client location not only depends on the direct path energy but also on the energy that is received from other directions due to reflections and multipath scattering. Depending on whether the resulting effect is constructive or destructive, the received signal strength can increase or decrease. This reduces the gap in beamforming gain between the *PAFD* and the DFT based codebook.

SI Reduction. In a multipath rich environment, the power of the nLoS component of the SI channel increases compared to an outdoor environment. This increases the SI in both *PAFD* (*PAFD* primarily reduces the power of the LoS component of the SI channel) and the DFT codebook.

Fig. 4(b) depicts the reduction in SI for a 4Tx-4Rx phased array antenna setup. With the DFT codebook, the average reduction in SI drops from 14.6 dB in the outdoor setup (Fig. 3(e)) to 12.8 dB in the indoor setup. In *PAFD*, the average reduction in SI drops from 41.4 dB in the outdoor setup (Fig. 3(e)) to 37.4 dB in the indoor setup.

Findings: The strong nLoS components of the SI channel in an indoor environment, increase the SI. However, PAFD can still provide large amounts of reduction in SI. Further, due to reflections and multipath scattering the gap in beamforming gain between PAFD and the DFT codebook decreases.

E. Capacity Gains Over Half-Duplex

In the previous sections, we observed that *PAFD* reduces the SI in the Rx phased array by accepting some loss in the beamforming gain. In this section, we compare the capacity

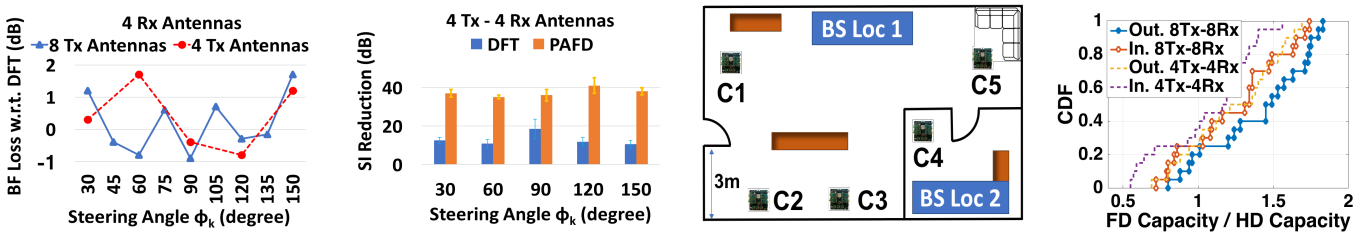

(a) (b) (c) (d)

Fig. 4. **(a): *PAFD*'s beamforming loss with respect to the DFT codebook in an indoor environment, (b): Indoor SI results for a 4Tx-4Rx antenna setup, (c): Layout of the indoor capacity evaluation experiments, (d): CDF of *PAFD*'s capacity gain to a HD system that employs the DFT codebook.**

gains that *PAFD* can deliver compared to a HD system that employs the DFT beams.

Scenario. We deploy 5 single antenna clients around the BS. All clients have connectivity to the BS, while some of them can be hidden from each other. We instruct the BS to sequentially transmit preambles across its DFT Tx beams. Each client finds the DFT beam index that achieves the highest SNR and sends the index back to the BS (*i.e.*, host PC in the WARPLab framework). Next, clients sequentially transmit preambles while the BS scans its DFT Rx beams (we set the weights of the DFT Rx beams similar to the DFT Tx beams). For each client, the BS selects the highest SNR achieving Rx DFT beam for its UL reception. We take the same steps to find the best Tx and Rx *PAFD* beams for each client.

Next, we sequentially go through all 10 possible combinations of selecting 2 clients out of all the 5 clients. For each selected pair, we randomly assign one client to the UL mode and the other one to the DL mode. We first let the system operate in HD mode and measure the UL and DL SNR values and the corresponding capacities. Let $C_{i,j}^{HD}$ denote the average HD capacity for client pair (i, j). Next, we let the system operate in FD mode and measure the UL and DL SINR values at the BS and the DL client, respectively. Note that the residual SI at the BS and the interference caused by the UL client on the DL client are accounted for in our FD SINR measurements. Let $C_{i,j}^{FD}$ denote the corresponding FD capacity.

We repeat these sets of experiments in both indoor and outdoor environments and with different numbers of antennas in our Tx and Rx phased arrays. For each environment and antenna setup, we do the experiments for two different BS locations to sufficiently sample the propagation environment. Fig. 4(c) depicts the layout of the indoor setup.

In our implementation of *PAFD*, we observed only 4-5 dB of SI above the noise floor. This remaining SI is due to the multipath components and can be suppressed by employing conventional digital cancellation techniques [5], [10]. However, given the remaining small margin for SI suppression with WARP, we do not consider it in our implementation. Thus our results would be a lower bound on *PAFD*'s performance.

Capacity Gains. Fig. 4(d) plots the CDF of all the $\frac{C_{i,j}^{FD}}{C_{i,j}^{HD}}$ values across all client pairs and BS locations. We consider both 4Tx-4Rx and 8Tx-8Rx antenna setups. The CDF plots with 4Tx-4Rx antenna setup are depicted through dashed lines, whereas the CDF plots of 8Tx-8Rx antenna setup are shown through solid lines with diamond markers.

According to the results shown in Fig. 4(d), *PAFD* achieves the best performance with an 8Tx-8Rx antenna setup in an outdoor environment. The low residual SI and the small beamforming gain loss compared to the DFT codebook, along with the FD operation result in high performance even in presence of UL to DL interference (interference caused by the UL client on the DL client's reception). We observe that in this setup, *PAFD* achieves a better performance than the HD system for 80% of the realizations.

In contrast, the SI reduction gains of *PAFD* reduce with a less number of antennas. This, coupled with more UL to DL interference in our indoor multipath rich environment, results in the least desirable performance when we have a 4Tx-4Rx antenna setup in the indoor environment. We observe that with this configuration, *PAFD* achieves a better performance than the HD system for 60% of realizations.

Findings: PAFD provides high capacity gains compared to a HD system in single cell environments even in presence of interference caused by UL clients to the DL clients. The gains increase with a larger array size and/or with less multipath.

F. Extension to Multiple Tx and Rx Phased Arrays (MIMO)

So far in our experiments we assumed a single Tx phased array and a single Rx phased array. We now evaluate the performance of *PAFD* with multiple Tx and Rx phased arrays. We first evaluate the reduction in SI when standard MU-MIMO techniques are used to communicate to two DL clients, while analog beams are selected according to *PAFD*. Next, we evaluate the capacity gains of FD-MIMO to HD-MIMO.

Scenario. We consider the deployment setup and measurement methodology that was discussed in the previous section (Section VI-E). However, our BS is equipped with 2 Tx phased arrays and 2 Rx phased arrays. Each phased array is equipped with 4 antennas and all the antennas are deployed in the ULA setup of Fig. 3(a). *PAFD* derives the analog beamformers of each Tx phased array based on its 4 Tx antennas and all the 8 Rx antennas. Similar to Section VI-E, we use the same set of Tx phase shifts for our Rx beams. We obtain the channel information to each client by sending a preamble on its selected beam. We consider all 5 possible combinations of selecting 4 clients out 5 and randomly select 2 of them for DL and the other 2 for UL. We employ the standard zero-forcing algorithms to communicate to 2 DL and 2 UL clients. We first conduct experiments to measure the reduction in SI at each Rx

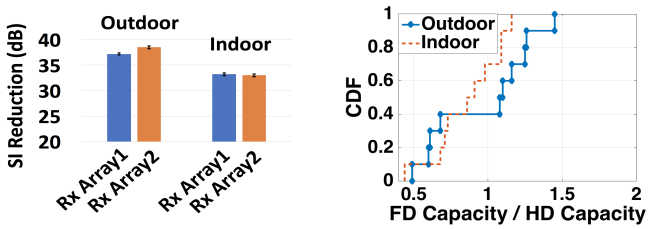

(a) (b)

Fig. 5. **MIMO experiments with 2 Tx phased arrays and 2 Rx phased arrays. There are 4 antennas on each Tx/Rx phased array. Standard zero-forcing is used for MU-MIMO to 2 DL clients and 2 UL clients. (a): Average reduction in SI across the antennas of each Rx phased array in indoor and outdoor environments; (b): Capacity gain of FD-MIMO to HD-MIMO in indoor and outdoor environments.**

phased array. Next, we conduct MU-MIMO experiments and measure the DL and UL SINR values for each client.

SI Reduction. Fig. 5(a) shows the reduction in SI at each of the two Rx phased arrays in both indoor and outdoor environments. We observe that outdoors, the average level of SI drops from 41.4 dB (in the 4Tx-4Rx setup of Fig. 3(e)) to 37.8 dB (*i.e.*, a drop of 3.6 dB). In the indoor environment, the average level of SI drops from 37.4 dB (in the 4Tx-4Rx setup of Fig. 4(b)) to 33 dB (*i.e.*, a drop of 4.4 dB). Note that an extra Tx phased array increases the noise power at the Rx phased array by an average of 3 dB. This, combined with a higher number of total Rx antennas (8 as opposed to 4 in the 4Tx-4Rx antenna setup of Fig. 3(e)), increases the SI.

Capacity Gains. Fig. 5(b) plots the CDF of the ratio of all the FD MU-MIMO capacities to their corresponding HD MU-MIMO capacities, across all client selections and the two BS locations. Similar to the SISO results (Fig. 4(d)), we observe that *PAFD* achieves a higher performance in the outdoor environment. However, *PAFD* achieves a higher capacity in only 60% of the realizations. Even though *PAFD* provides large amounts of reduction in SI power in the MIMO setup, there is more interference due to having a higher number of UL clients. Recent works have proposed scheduling and cancellation algorithms to eliminate the UL to DL interference (*e.g.*, [25]). We can leverage these techniques in *PAFD* to remove UL to DL interference and close to double the spectral efficiency of HD MU-MIMO hybrid beamforming systems.

Findings: PAFD scales to multiple Tx and Rx phased arrays, enabling MIMO FD in hybrid beamforming systems with phased array antennas. Further, PAFD is agnostic of the underlying baseband beamforming and can operate on the output of such algorithms (e.g., DL / UL MU-MIMO).

VII. Conclusions

We presented the design and implementation of *PAFD*, a design methodology that enables FD in hybrid beamforming systems with phased array antennas. We proposed an analog beamformer design problem formulation that simultaneously maximizes the beamforming gain in the desired direction and reduces the overall SI power. We also proposed a semidefinite programming relaxation to solve this problem. We implemented *PAFD* on the WARP platform, and showed that compared to the standard DFT beams that maximize the beam gain in the desired directions, *PAFD* provides large amounts of SI reduction with minimal impact to the beamforming gain.

References

[1] J. Choi, M. Jain, K. Srinivasan, P. Levis, and S. Katti, "Achieving single channel, full duplex wireless communication," in *Proceedings of ACM MOBICOM*, 2010.

[2] M. Jain, T.M. Kim, D. Bharadia, S. Seth, K. Srinivasan, P. Levis, S. Katti, and P. Sinha, "Practical, real-time, full duplex wireless," in *Proceedings of ACM MOBICOM*, 2011.

[3] E. Aryafar, M.A. Khojastepour, K. Sundaresan, S. Rangarajan, and M. Chiang, "MIDU: enabling mimo full duplex," in *Proceedings of ACM MOBICOM*, 2012.

[4] E. Everett, A. Sahai, and A. Sabharwal, "Passive self-interference suppression for full-duplex infrastructure nodes," in *IEEE Transactions on Wireless Communications*, 2013.

[5] D. Bharadia, E. McMilin, and S. Katti, "Full duplex radios," in *Proceedings of ACM SIGCOMM*, 2013.

[6] "3GPP TR 38.802; 3rd generation partnership project; technical specification group radio access network; study on new radio (NR) access technology; physical layer aspects (release 14)," 2017.

[7] E. Aryafar, N. Anand, T. Salonidis, and E. Knightly, "Design and experimental evaluation of multi-user beamforming in wireless LANs," in *Proceedings of ACM MOBICOM*, 2010.

[8] C. A. Balanis, "Antenna theory: analysis and design (3rd ed.)," John Wiley, 2005.

[9] "Anokiwave 28 GHz phased array," Product description available at: http://www.anokiwave.com/products/awmf-0129/index.html.

[10] M. Duarte, C. Dick, and A. Sabharwal, "Experiment-driven characterization of full-duplex wireless systems," in *IEEE Transactions on Wireless Communications*, 2012.

[11] C. Shepard, H. Yu, N. Anand, E. Li, T. Marzetta, R. Yang, and L. Zhong, "Argos: practical many-antenna base stations," in *Proceedings of ACM MOBICOM*, 2012.

[12] Q. Yang, X. Li, H. Yao, J. Fang, K. Tan, W. Hu, J. Zhang, and Y. Zhang, "Bigstation: enabling scalable real-time signal processing in large mu-mimo systems," in *Proceedings of ACM SIGCOMM*, 2012.

[13] X. Xie, E. Chai, X. Zhang, K. Sundaresan, A. Khojastepour, and S. Rangarajan, "Hekaton: efficient and practical large-scale mimo," in *Proceedings of ACM MOBICOM*, 2015.

[14] E. Everett, C. Shepard, and A. Sabharwal, "SoftNull: many-antenna full-duplex wireless via digital beamforming," in *IEEE Transactions on Wireless Communications*, 2016.

[15] H. Lebret and S. Boyd, "Antenna array pattern synthesis via convex optimization," in *IEEE Transactions on Signal Processing*, 1997.

[16] L. Guo, H. Deng, B. Himed, T. Ma, and Z. Geng, "Waveform optimization for transmit beamforming with mimo radar antenna arrays," in *IEEE Transactions on Antennas and Propagation*, 2015.

[17] H. He, P. Stoica, and J. Li, "Wideband mimo systems: signal design for transmit beampattern synthesis," in *IEEE Transactions on Signal Processing*, 2011.

[18] A. J. Fenn, "Evaluation of adaptive phased array antenna, far-field nulling performance in the near-field region," in *IEEE Transactions on Antennas and Propagation*, 1990.

[19] S. S. Sussman, "Least-square synthesis of radar ambiguity functions," in *IRE Transactions on Information Theory*, 1962.

[20] M. Fazel, H. Hindi, and S. Boyd, "Rank minimization and applications in system theory," in *Proceedings of IEEE American Control Conference*, 2004.

[21] G. Strang, "Introduction to linear algebra (4th ed.)," Wellesley Cambridge Press, 2009.

[22] "Results on zero-forcing mu-mimo," Freescale Semiconductor Inc., 3GPP TSG RAN WG1, R1-071511, Technical Repport, 2007.

[23] A. Alkhateeb, O. E. Ayach, G. Leus, and R. W. Heath, "Channel estimation and hybrid precoding for millimeter wave cellular systems," in *IEEE Journal of Selected Topics in Signal Processing*, 2014.

[24] A. S. Y. Poon, R. W. Brodersen, and D. N. C. Tse, "Degrees of freedom in multiple-antenna channels: a signal space approach," in *IEEE Transactions on Information Theory*, 2005.

[25] A. Bai and A. Sabharwal, "Distributed full-duplex via wireless side-channels: bounds and protocols," in *IEEE Transactions on Wireless Communications*, 2013.